Research Article

ADVANCED PHOTONICS

Wavefront-selective Fano resonant metasurfaces

Adam Overvig[a] **and Andrea Alù**[a,b,*]

[a]City University of New York, Advanced Science Research Center, Photonics Initiative, New York, United States
[b]City University of New York, Graduate Center, Physics Program, New York, United States

Abstract. Fano resonances are conventionally understood as sharp spectral features with selectivity in the momentum-frequency domain, implying that they can be excited only by plane waves with specific frequencies and incident angles. We demonstrate that Fano resonances can be made generally selective in the space-frequency domain. They can be tailored to resonate only when excited by a frequency, polarization, and wavefront of choice. This generalization reveals that Fano systems are characterized by eigenwaves that scatter to their time-reversed image upon reflection. Although in conventional Fano systems this trivially occurs for normally incident plane waves, we show that, in general, the selected wavefront is locally retroreflected everywhere across the device. These results show that conventional Fano resonances are a subset of a broader dichroic phenomenon with spin, spatial, and spectral selectivity. We demonstrate these concepts with nonlocal metasurfaces whose governing principles are deeply rooted in the symmetry features of quasi-bound states in the continuum. Enhanced light–matter interactions and symmetry-protection make these phenomena uniquely suited for enriching applications in quantum optics, non-linear optics, augmented reality, and secure optical communications, laying the groundwork for a range of novel compact optical sources and devices.

Keywords: nonlocal metasurface; Fano resonance; spatial selectivity; quasi-bound states in the continuum.

Received Nov. 17, 2020; accepted for publication Mar. 1, 2021; published online Mar. 18, 2021.

[DOI: 10.1117/1.AP.3.2.026002]

1 Introduction

Optical Fano resonance is a phenomenon born of interference between a discrete (dark) state and a broad (bright) continuum of states. Observed in many photonic systems,[1] it is characterized by an asymmetric lineshape originally described by Fano in 1961.[2] Wood's anomaly is a prominent early example of such a phenomenon, wherein sharp resonant features were observed in the spectra of super-wavelength metallic gratings at discrete angles and frequencies at which diffractive orders emerge.[3,4] Modern micro- and nano-technology has enabled subwavelength patterning of surfaces that exhibit more complex Fano resonant responses. For instance, in weakly corrugated dielectric slabs, weak coupling of light to a discrete waveguide mode can interfere with strong coupling to a broadband thin-film resonance, enabling a guided mode resonance.[5] Such devices behave as notch filters, selective to a specific combination of angles and frequencies that track the dispersion of the underlying waveguide mode.[6,7] Similar responses are observed in photonic crystal slabs and strongly corrugated gratings,[8] well-modeled by temporal coupled mode theory that can accurately predict the Fano lineshape.[9]

In specific cases, the linewidth of these resonant modes may vanish in such periodic systems, implying that their radiative lifetime becomes infinite and the mode becomes a bound state in the continuum (BIC).[10,11] When this suppression of coupling to radiation is due to symmetry-protection,[12] applying a perturbation that breaks the relevant symmetry introduces radiative coupling, yielding a quasi-bound state in the continuum (q-BIC) responsible for a Fano resonance whose linewidth is directly controlled by the perturbation.[13,14] Due to their origin lying in symmetries, q-BICs are broadly applicable across many geometries and material systems and have been rapidly emerging as a powerful rationally designed platform leveraging enhanced-light–matter interactions[15] to advance planarized optical modulators,[16] biological sensors,[17] and compact non-linear optical devices.[18,19]

As with other Fano resonant systems, q-BICs have been commonly studied in infinitely periodic photonic crystal slabs with subwavelength periodicity, affording two notable simplifications: (i) the presence of a single diffraction order, into which the supported dark and bright modes may interfere, and (ii) a natural description in momentum-frequency space. In such

*Address all correspondence to Andrea Alù, aalu@gc.cuny.edu

systems, the peak reflectance is unity in the absence of optical loss,[20] a marker of complete interference between the bright and dark modes, and the Fano resonance can be observed only for incident plane waves matching the underlying band structure in both momentum (angular selectivity) and frequency (spectral selectivity). The polarization properties are governed by selection rules[14] that specify whether the excitation of a q-BIC may be forbidden or allowed according to the space group of the perturbed symmetry. Notably, a metasurface patterned in a way to retain only twofold rotation symmetries after perturbation, i.e., having a p2 space group, may couple a q-BIC to any designer linear polarization angle with arbitrary lifetime.[14,21] By introducing suitable out-of-plane symmetry-breaking perturbations, q-BICs can also extend circularly dichroic Fano resonances[22–25] to exhibit arbitrary elliptical dichroism.[26] These systems thereby exhibit rationally tailorable selectivity to polarization, momentum, and frequency rooted in symmetry breaking.

Recently, Fano resonant metasurfaces capable of shaping the wavefront of light at resonance have been demonstrated based on the symmetry features of q-BICs.[14,21,26–28] In Ref. 21, it was demonstrated that the orientable linear dichroism afforded by the p2 space group can carry a geometric phase when excited by circular polarization. The local response to a linear polarization of choice may, therefore, be spatially varied, locally imparting a controlled geometric phase due to scattering from the nonlocal q-BIC mode. As a result, aperiodic functionalities, such as frequency-selective focusing of incident light, can be demonstrated using this technique,[27,28] but with efficiencies fundamentally limited by the achirality of the underlying structure. Incident circular polarization is not the selected polarization state at any point across the surface; therefore, the functionality of these systems is afforded by an incomplete projection of the incoming polarization to the locally selected states. In Ref. 26, this limitation was addressed by introducing chiral perturbations that can select purely circularly polarized states. Here, the metasurface operation of interest can be implemented with unity efficiency by locally varying the orientation of the selected circular polarization (a degeneracy of the poles of the Poincaré sphere). Although this functionality was enabled only in strictly periodic structures in Ref. 26 so far, the earlier results demonstrating frequency selective wavefront-shaping based on linearly polarized q-BICs suggest that the usual description of these systems in the momentum-frequency domain is insufficient.

In this paper, we expand the concept of Fano resonant metasurfaces to sustain arbitrarily varying spatial profiles and arbitrary polarization states. We achieve this feature in aperiodic metasurfaces that exhibit the frequency selectivity of conventional Fano resonance metasurfaces and, at the same time, the wavefront-shaping functionality traditionally found in phase-manipulating metasurfaces based on geometric phase concepts.[29–33] At first glance, this combination of features is surprising and counterintuitive, because the former is a highly nonlocal phenomenon (the optical response at each position has significant contributions from distant positions), whereas the latter is explicitly conceived as enabled by a local response, ignoring interactions from other unit cells.[30] We resolve this apparent challenge by showing that the conventionally studied Fano metasurfaces, offering momentum-frequency selectivity, are a limited subset of a more general dichroic nonlocal phenomenon that supports space-frequency selectivity. In other words, we show that the chiral q-BICs introduced in Ref. 26 can establish a general platform for metasurfaces that fully resonate only for specific frequencies, incoming wavefronts, and polarization of choice. Due to their periodicity, the resonant wavefront in conventional Fano metasurfaces is limited to plane waves, whereas in our generalized form of Fano metasurfaces, we find that the selected wavefront can be arbitrarily tailored by symmetry breaking across the device. The selected wavefront of choice is resonantly transformed into its time-reversed copy upon reflection, implying that the reflection process preserves handedness in stark contrast to conventional specular reflection. Due to this property of preserving handedness, we name this wavefront the principal "eigenwave" of our Fano metasurfaces. We show that this eigenwave is the incident wavefront that excites the band-edge mode of the unperturbed periodic photonic crystal slab to which the spatial perturbation is applied, i.e., while different perturbation profiles establish distinct eigenwaves, in each case the eigenwave excites the same q-BIC mode profile. Based on these principles, we demonstrate metasurfaces offering unprecedented new functionalities: first, we show that in the case of a linear gradient of geometrical phase, the eigenwave is retroreflected with preserved spin angular momentum (SAM). Next, we demonstrate a chiral nonlocal metasurface lens that strongly reflects only when illuminated by a circularly polarized spherical wave originating from twice the focal distance. Finally, we show chiral q-BIC metasurfaces with azimuthally varying phase gradients, supporting a Fano resonance that is selective to the orbital angular momentum (OAM) of incident light. In this scenario, the eigenwave is a vortex beam reflected with preserved SAM and OAM. We finally discuss the implications of these findings for a variety of nanophotonic applications, from secure communications to thermal emission engineering.

2 Methods

To begin, we compare a conventional periodic Fano metasurface to the proposed aperiodic geometry. As noted above, a conventional periodic Fano device is known to support strong polarization and spectral and angular selectivity. Its resonant response is characterized by an eigenpolarization, which, in cases without birefringence, can be defined as the polarization for which (i) a maximum Fano resonant response is achieved and (ii) the reflected wave has the same polarization state, i.e., it is the eigenvector of the reflection-side Jones matrix with near-unity eigenvalue at resonance. As depicted in Fig. 1(a), when illuminated by normally incident light at resonance matching the eigenpolarization (limited to linear polarizations), a standing wave q-BIC, corresponding to the band-edge mode in reciprocal space, is excited everywhere across the device, and the incident wave is completely reflected. When illuminated by a spatially varying wavefront composed of many plane waves [Fig. 1(b)], the band-edge mode cannot be uniformly excited (if at all), the spectral resonance feature is lost, and little (if any) light is reflected.

In contrast, the proposed chiral aperiodic q-BIC metasurface introduced here supports a resonant mode with arbitrarily tailored spin, spectral, and wavefront selectivity. In this case [Fig. 1(c)], a designer wavefront excites with maximum efficiency the band-edge mode everywhere across the device, and light is reflected to an identical wavefront propagating in the opposite direction only for the chosen spin and resonant frequency. When excited by another wavefront, such as a plane wave at arbitrary incidence, the band-edge mode is not uniformly excited (if at all), the spectral feature is lost, and little (if any) light is reflected [Fig. 1(d)]. In the following, we outline the conditions to realize such an aperiodic metasurface supporting an incident wavefront of choice

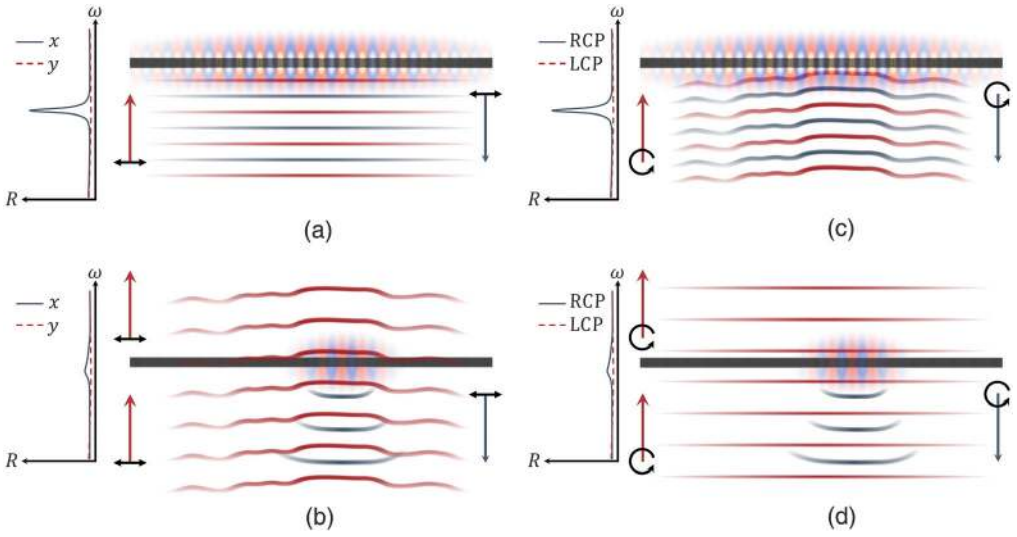

Fig. 1 Spin, spectral, and spatial selectivity in Fano metasurfaces. (a) A conventional Fano resonant metasurface with spectral and angular selectivity supports a band-edge mode that is maximally Fano resonant for *x* polarized light at normal incidence. (b) When an arbitrary wavefront is incident on it, no distinct spectral feature can be found, and the wave is primarily transmitted with little distortion. In this case, the band-edge mode is not excited. (c) Proposed metasurface with spin, spectral, and spatial selectivity, yielding a band-edge mode maximally Fano resonant for RCP light with a specifically tailored wavefront. (d) When an arbitrary plane wave is incident, no distinct spectral feature can be observed, and light is primarily transmitted with little distortion.

that is (i) maximally Fano resonant and (ii) reflected with preserved handedness.

Before demonstrating aperiodic devices, we begin by numerically studying the eigenwaves in the simplest case of a periodic phase gradient Fano metasurface. In order to design the structure, we use the unit cells introduced in Ref. 26, which are discussed in more detail in Sec. S1 in the Supplemental Materials. In particular, we consider metasurfaces comprising two stacked planarized layers with chiral perturbations in their unit cells, and we compare the case without a spatial phase gradient of these perturbations [Fig. 2(a)], serving as a reference case, and the case with a gradient in the x direction [Fig. 2(b)]. Sitting on a substrate with $n_1 = 1.45$, the metasurfaces are realized in thin films with $n_2 = 3.45$ etched by elliptical holes with dimensions of $80\,\text{nm} \times 340\,\text{nm}$ spaced with pitch of $a = 400\,\text{nm}$. The ellipses are filled with the superstrate material, $n_3 = n_1$. As shown in Fig. 2(c), each unit cell has two ellipses per layer: in the first layer, they are oriented by angles α and $\alpha + 90$ deg, whereas, in the second layer, they are oriented by angles $\alpha + \Delta\alpha$ and $\alpha + \Delta\alpha + 90$ deg. Section S1 in the Supplemental Materials provides additional details on the rationale for this unit cell geometry and for their characterization. Although our focus here is on the expansion of the theoretical concept of Fano resonant metasurfaces, we emphasize that the fabrication of this planarized layer stack is compatible within standard nano-fabrication techniques at optical frequencies[31,32] or standard approaches in the microwave regime.[34] We propose a possible fabrication procedure in Sec. S2 in the Supplemental Materials based on extending recent efforts demonstrating single-layer q-BIC metasurfaces,[19,27,28] and we study the influence of misalignment of the two layers in Sec. S3 in the Supplemental Materials, concluding that standard tolerances more than suffice to demonstrate these concepts in the near-infrared.

As shown in Ref. 26, in the unit cell of Fig. 2, $\Delta\alpha$ controls the chirality of the optical response, whereas α controls a geometric phase that varies as 4α. Generally, $\Delta\alpha$ and α may be tuned to achieve arbitrary elliptical eigenpolarization in the form

$$|e\rangle = \begin{bmatrix} \cos(\psi) & -\sin(\psi) \\ \sin(\psi) & \cos(\psi) \end{bmatrix} \begin{bmatrix} \cos(\chi) \\ i\,\sin(\chi) \end{bmatrix}, \tag{1}$$

where 2χ is the latitude, and 2ψ is the longitude on the Poincaré sphere. These metasurfaces support a Fano resonance that reflects its eigenpolarization to a state proportional to $|e^*\rangle$, with near-unity peak reflectance. In particular, $\Delta\alpha \approx 45$ deg yields $2\chi = \pi/2$, whereas the other elliptical parameter varies as $\psi \approx 2\alpha$. In this case, we have a q-BIC right-handed circularly polarized (RCP) eigenpolarization:

$$|e\rangle = e^{i2\alpha}|R\rangle = \frac{e^{i2\alpha}}{\sqrt{2}} \begin{bmatrix} 1 \\ i \end{bmatrix}. \tag{2}$$

The q-BIC at the band-edge frequency is a quasi-TE mode characterized by an out-of-plane magnetic field $H_z^0(x, y)$, where the superscript specifies the mode profile in the absence of perturbation, i.e., the band-edge mode of the underlying high-symmetry photonic crystal slab (see Sec. S1 in the Supplemental Materials). Due to the symmetry-breaking perturbation, this mode couples out to free-space light with a state:

$$\langle e|R\rangle^2 |R^*\rangle = e^{i4\alpha}|R^*\rangle. \tag{3}$$

A spatially varying $\alpha(x, y)$ results in a device that anomalously reflects normally incident plane waves only for the resonant frequency.[26]

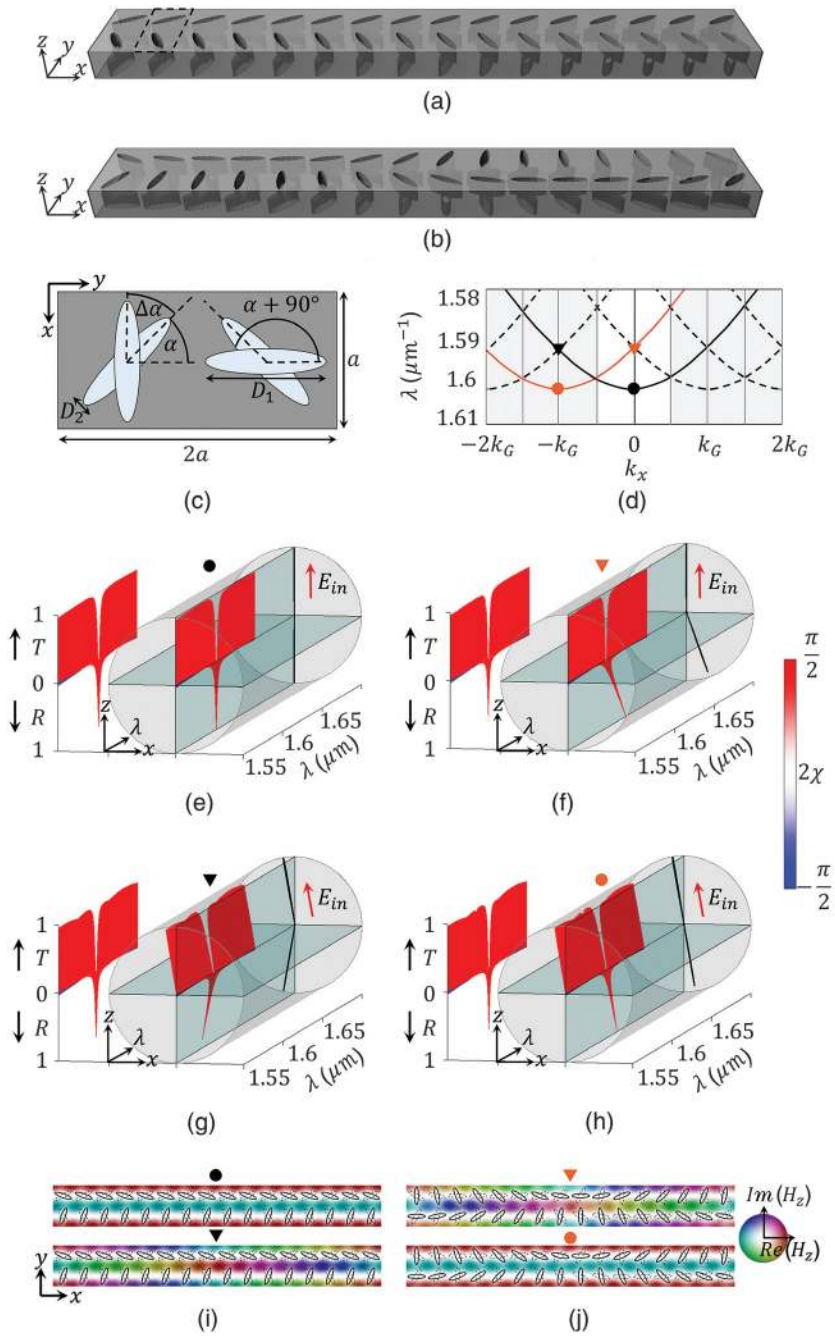

Fig. 2 Eigenwaves of linear phase gradient resonant metasurfaces. (a), (b) Schematics of chiral PCSs without and with a phase gradient. The substrate and superstrate are omitted for clarity. (c) Top view of a chiral meta-unit of the devices [dashed rectangle in (a)]. (d) Band diagrams: the solid black band refers to the device in (a) and the solid orange band for (b). Black and orange markers denote the devices in (a) and (b), and circles denote the eigenwaves. (e)–(h) Far-field projections near the resonant wavelengths for incident RCP plane waves with momenta marked in (d). The anomalous reflection in (f) is to an angle of 20.1 deg, and the incident angle for (g) and (h) is 9.89 deg (half the momentum of the anomalous reflection). The color map tracks 2χ of the output polarization state, demonstrating that light resonantly reflects with preserved spin. When the eigenwave (e), (h) is incident, retroreflection occurs, indicating preservation of handedness. (i), (j) Field profiles on the resonance for each case [fields are shown at the bottom interface of the devices in (a) and (b)].

Next, we consider a general incident RCP wavefront traveling in the z direction with spatially varying amplitude $A(x,y)$ and phase $\Phi_{\text{in}}(x,y)$:

$$E_{\text{in}}(x,y) = A(x,y)e^{i\Phi_{\text{in}}(x,y)}e^{ik_z z}|R\rangle, \tag{4}$$

where we assume adiabatic spatial variations relative to the scale of the pitch a of the metasurface and use $-i\omega t$ time dependence. This wave is incident on a device with spatially varying perturbation $\alpha(x,y)$, coupling into the q-BIC modulated by the input field profile and the coupling factor in Eq. (2):

$$H_z(x,y) = H_z^0(x,y)A(x,y)e^{i\Phi_{\text{in}}(x,y)}e^{i2\alpha(x,y)}. \tag{5}$$

This mode then couples to free space, creating an outgoing wavefront:

$$E_{\text{out}}(x,y) = A(x,y)e^{i\Phi_{\text{in}}(x,y)}e^{i4\alpha(x,y)}e^{-ik_z z}|R^*\rangle. \tag{6}$$

Next, we choose $2\alpha(x,y) = -\Phi_{\text{in}}(x,y)$, implying that the incident phase profile precisely cancels the phase encoded by the device. The resulting field profile of the q-BIC is

$$H_z(x,y) = H_z^0(x,y)A(x,y). \tag{7}$$

In other words, the q-BIC has a field profile that is simply the unperturbed field profile modulated by the amplitude envelope of the incident wavefront. Meanwhile, the outgoing field profile is

$$E_{\text{out}}(x,y) = A(x,y)e^{-i\Phi_{\text{in}}(x,y)}e^{-ik_z z}|R^*\rangle = E_{\text{in}}^*(x,y). \tag{8}$$

Hence the output wavefront is the time-reversed copy of the input wavefront, and E_{in} is the eigenwave of the q-BIC metasurface. Interestingly, with this strategy, we can pattern arbitrary wavefronts into becoming the eigenwaves of our Fano metasurface, with exciting opportunities for augmented reality and secure communications, since the response of interest is excited exclusively when the specific spin, frequency, and wavefront distribution illuminates the metasurface. In the following, we confirm these predictions by numerically studying the metasurfaces in Figs. 2(a) and 2(b) when illuminated by two plane waves, each an eigenwave of one of the devices. We then apply these ideas to metalenses and vortex-beam metasurfaces. We use the full-wave finite difference time domain method (Lumerical Solutions) for all numerical results in this work.

3 Results

As shown in Fig. 2(d), the band structure of a nonlocal metasurface encoded with a phase gradient (see Sec. S1 in the Supplementary Material) contains zone-folded copies of the band structure of the dimer in Fig. 2(c) (solid black curve) at intervals of $k_G = \pi/8a$, consistent with the superperiod $16a$. Since the device in Fig. 2(a) has no variation across its metaunits, its band structure is identical to the dimer. In this reference case, the eigenwave is unsurprisingly the plane wave at normal incidence, marked by a black circle on the band diagram. The black circle is at the edge of a band we may approximate parabolically as

$$\omega_{\text{res}}(k_x) = \omega_0 + \frac{b}{2}k_x^2, \tag{9}$$

where ω_0 is the band-edge frequency, and b is a measure of the band curvature near $k_x = 0$. The far-field optical response due to light at normal incidence from the substrate side is seen in Fig. 2(e), showing direct reflection of the resonant light with the same RCP polarization state (red). In contrast, the non-resonant light (which mostly transmits) reflects with inverted spin (blue), as expected. The q-BIC field profile is simply $H_z^0(x,y)$, as shown in Fig. 2(i). (Note that throughout we depict these field profiles at the bottom interface of each device.)

However, the device in Fig. 2(b) encodes a phase gradient:

$$\frac{\partial\Phi(x,y)}{\partial x} = 4\frac{\partial\alpha(x,y)}{\partial x} = +2k_G, \tag{10}$$

meaning that normally incident light is anomalously reflected to an angle of 20.1 deg in the substrate [Fig. 2(f)]. Per Eqs. (5) and (10), the q-BIC now has the eigenfield profile:

$$H_z(x,y) = H_z^0(x,y)e^{ik_G x}. \tag{11}$$

In other words, the mode profile is modulated by the Bloch wavevector $+k_G$ contributed by the phase gradient [Fig. 2(j)]. Its resonant frequency follows the relation [Eq. (9)] shifted by the Bloch wavevector:

$$\omega_{\text{res}}(k_x) = \omega_0 + \frac{b}{2}(k_x + k_G)^2. \tag{12}$$

Comparing Eqs. (7) and (11), the eigenwave of the device in Fig. 2(b) must cancel this exponential factor, and so it must be a planewave with wavevector $-k_G$ and frequency ω_0.

Figure 2(g) shows the optical response of the reference device [Fig. 2(a)] due to illumination by this off-normal plane wave, showing specular reflection, as expected. The q-BIC mode profile is simply

$$H_z(x,y) = H_z^0(x,y)e^{-ik_G x}, \tag{13}$$

as shown in Fig. 2(k). This mode is marked by a black triangle in the band diagram in Fig. 2(d), showing a resonant frequency shift that follows the angular dispersion of the band [Eq. (9)]. In contrast, when the same plane wave is incident onto the metasurface in Fig. 2(b), from Eq. (6), we find

$$E_{\text{out}}(x,y) = e^{-ik_G}e^{i2k_G}e^{-ik_z z}|R^*\rangle = e^{ik_G}e^{-ik_z z}|R^*\rangle, \tag{14}$$

implying that resonant light is retroreflected [Fig. 2(h)] with preserved spin. Non-resonant light is specularly reflected with inverted spin, as expected. Figure 2(l) shows that the q-BIC mode profile is indeed $H_z^0(x,y)$, consistent with Eq. (7). Since this mode is excited by wavevector $-k_G$, but is identical to the one marked by the black circle in Fig. 2(d), it corresponds to the mode marked by an orange circle in Fig. 2(d). That is, the eigenwave excites the band-edge mode of the band (solid orange) translated by the eigenwave wavevector $-k_G$ [Eq. (12)]. Finally, the mode in Fig. 2(j) is shifted by $+k_G$ and is marked by the orange triangle.

Although the periodic metasurface in Fig. 2(b) has a specific value of k_G, the same response may be achieved for an arbitrary

choice of k_G by varying the gradient phase profile, or, more generally, we may envision aperiodic metasurfaces, in which k_G spatially varies across the device. The eigenwave in all cases will excite the band-edge q-BIC with a negligible resonant frequency shift with respect to the reference case in Fig. 2(a). We demonstrate this interesting feature in a resonant metasurface lens[21] with focal length $\sim f/2$, encoded by the phase profile:

$$\frac{\partial \Phi(x,y)}{\partial x} = 4\frac{\partial \alpha(x,y)}{\partial x} = -2k_0 \frac{x}{\sqrt{x^2+f^2}}. \tag{15}$$

The eigenwave in this case, per Eq. (4), becomes

$$E_{\text{in}}(x,y) = e^{ik_0\sqrt{x^2+f^2}} e^{ik_z z}|R\rangle, \tag{16}$$

which is simply an RCP spherical wave originating at $z_0 = f$. Figure 3(a) shows the intensity of a spherical wave emanating from an ideal point source at a position $z_0 = 425$ μm. The metasurface is placed at $z = 0$ and encoded with the phase profile in Eq. (15) with $f = 425$ μm, which corresponds to a lens focusing light incident at normal incidence with a numerical aperture NA ≈ 0.5, defined here as $\text{NA} = n_1 \frac{W/2}{\sqrt{(W/2)^2+(f/2)^2}}$ for a lens of width W. The reflected light due to this excitation is shown in Fig. 3(b) at the resonant frequency, showing refocusing of the light to the original point source position. The reflectance due to this excitation is shown in Fig. 3(c) both for an RCP and left-handed circularly polarized (LCP) spherical waves, showing near-unity reflectance when excited by the RCP eigenwave. This reflectance is calculated by integrating (as a function of space) the total power reflected off the surface, passing through a plane placed at $z = 2$ μm, and then normalizing the result to the incident power falling on the metasurface. The phase profile Φ_{in} arriving at the metasurface is shown in Fig. 3(d) along with the reflected phase profile at resonance Φ_{out} and modal phase profile Φ_{mode} (sampled at positions along the bottom plane of the device at $y = 0$), which follow closely the predicted forms [Eqs. (7) and (8), respectively]. Figure 3(e) shows the mode field profile at two locations along the lens, showing the band-edge mode profile as expected, but with small residual phase deviations tracked in Fig. 3(d). Note that this slow phase drift indicates a slight deviation from the ideal eigenwave condition [Eq. (7)], but, in comparison to the encoded phase profile, it is very small. This deviation, together with the reflectance in Fig. 3(c) not peaking at unity and the reflected phase profile in Fig. 3(d) not matching a perfect hyperbola, is due to the imperfections in the metasurface implementation and the non-ideal adiabaticity of the geometric phase variations across the surface. Yet, despite these non-idealities, the agreement conceptually is excellent with our theoretical model: the eigenwave locally cancels the encoded phase gradient and resonantly reflects to a phase-conjugated copy of itself with near-unity reflectance via interference with a q-BIC, whose essential features are those of the band-edge mode.

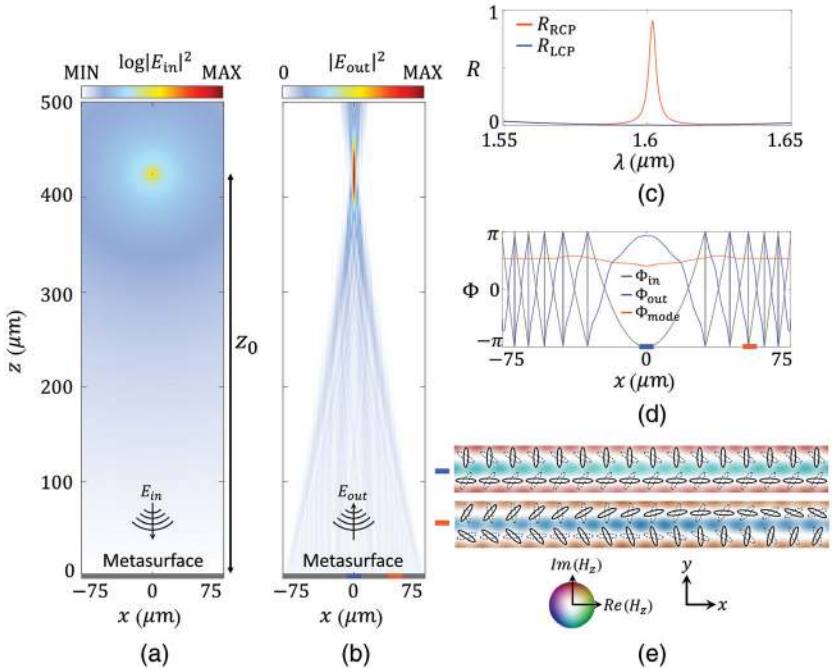

Fig. 3 Eigenwave of a q-BIC metasurface forming a converging lens. (a) Field intensity (log scale) for an ideal point source placed along the optical axis $x = 0$ at a distance $z_0 = 425$ μm from the metasurface. (b) Intensity (linear scale) of reflected light when the metasurface is encoded such that the field in (a) is the eigenwave. (c) Reflectance when the point source in (a) is RCP and LCP, calculated by summing the reflected power at a plane 2 μm above the metasurface and normalizing to the power in (a) that falls on the metasurface. (d) Input, output, and mode phase profiles at the eigenwave condition. (e) Mode profile at the eigenwave condition at two locations along the lens, demonstrating that the eigenwave excites the band-edge mode at a near-constant phase across the device.

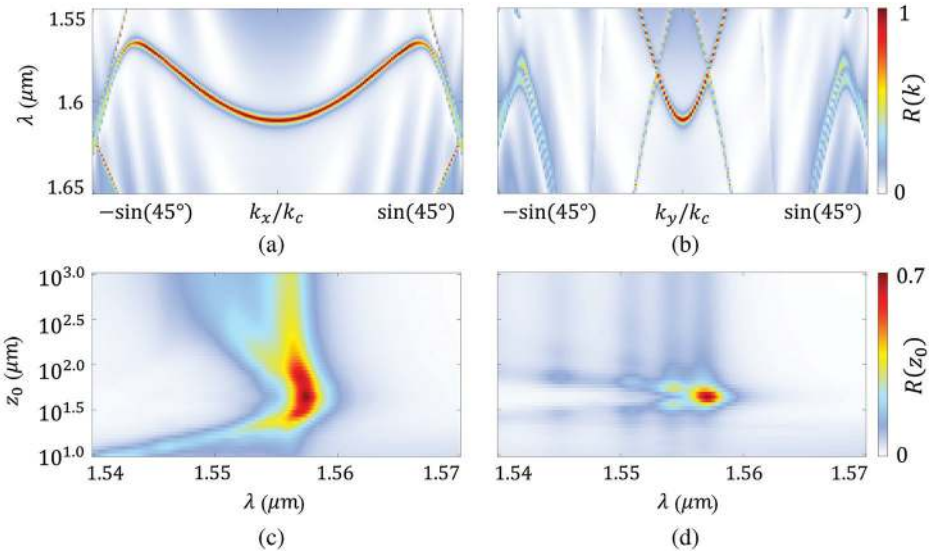

Fig. 4 Spatial selectivity and band curvature. (a), (b) Reflectance in the case of a uniform phase profile along the k_x and k_y directions. (c), (d) Reflectance of metasurface lenses (such as in Fig. 3) with widths of $W = 50$ μm focusing in the x and y directions, due to RCP point sources placed at various positions z_0 along the optical axis. The case of (d) is shown with substantial spatial selectivity in comparison to (c), corresponding to the sharper band structure in the k_y direction (b) in comparison to that in the k_x direction.

Next, we demonstrate the spatial selectivity of our metasurface by studying how the reflectance depends on the location of the point source z_0. The spatial selectivity of the metasurface implies that maximal reflectance is achieved only when the eigenwave is incident from ($z_0 = f$) and the reflectance drops as z_0 changes. We verify this prediction in two scenarios, when the phase function is applied along the x direction [for which the q-BIC has the flat band structure seen in Fig. 4(a)] and when the phase function is applied along the y direction [for which the q-BIC has the sharper band structure seen in Fig. 4(b)]. The reflectance due to RCP waves emitted from positions z_0 is shown in Figs. 4(c) and 4(d) for metasurface lenses of widths $W = 50$ μm and identical NA ≈ 0.48 to the device in Fig. 3. The results show maximal reflectance only at the eigenwave condition and reduced reflectance as the excitation moves away from the optimal location.

Notably, the reflectance drop-off is drastically different in the two cases, implying a different wavefront selectivity for the two planes. This difference is explained by the physical origin of the spatial selectivity: the resonant frequency shifts according to the local phase gradient. As shown in Fig. 2(d), the q-BIC band shifts in k-space by an amount k_G following Eq. (10). If the phase gradient changes adiabatically, we may view each section of the lens as approximated by such a band structure, wherein the shift k_G increases in magnitude away from lens center following Eq. (15). For light at normal incidence, for instance, this band shift corresponds to a distinct resonant frequency shift at the various positions across the device following Eq. (12), but with k_G being a function of x. This means that light at normal incidence does not excite the band-edge mode everywhere across the device simultaneously, and the spectral response is lost [as depicted in Fig. 1(d)]. In contrast, the eigenwave represents the specific wavefront for which everywhere across the device this shift is precisely canceled, i.e., it is the wave whose local momentum exactly counters the k-space shift imprinted on the surface and excites the band-edge mode at frequency ω_0 everywhere across the device. Therefore, our nonlocal metalens owes its spatial selectivity to the resonant dispersion of the underlying q-BIC. The flatter the band is, the smaller the shift in resonant frequency for the same magnitude of phase gradient is, and the smaller the spatial selectivity is. Likewise, a lower Q-factor implies that a larger frequency shift may be tolerated before the spectral feature is lost. Therefore, for large dispersion and high Q-factors, only incident waves closely matching the eigenwave exhibit any appreciable Fano spectral feature, and we see that the spatial selectivity is a natural consequence of the momentum selectivity in the periodic geometry.

Finally, we study a nonlocal metasurface with

$$\Phi(x, y) = 2m \arctan 2(y, x), \tag{17}$$

where m is an integer. It is easy to see that the metasurface in this case will be selective to a vortex beam with OAM $\ell = -m$:

$$E_{\text{in}}(x, y) = A_0(x^2 + y^2)^{|\ell|/2} e^{-(x^2+y^2)/w_0^2} e^{i2\ell \arctan 2(y,x)} e^{ik_z z} |R\rangle, \tag{18}$$

where w_0 is the beam waist, and A_0 determines the field strength. We spatially vary the orientation angle according to

$$\alpha(x, y) = m \arctan 2(y, x), \tag{19}$$

with $m = -1$. The eigenwave becomes a vortex beam following Eq. (18) with $\ell = 1$. Due to computational constraints, we limited the size of the simulated device to 30 μm $\times$ 30 μm and chose $w_0 = 7$ μm to keep the optical power well-contained within the boundaries of the device. The amplitude and phase of the incident field are shown in Fig. 5(d), along with a table summarizing

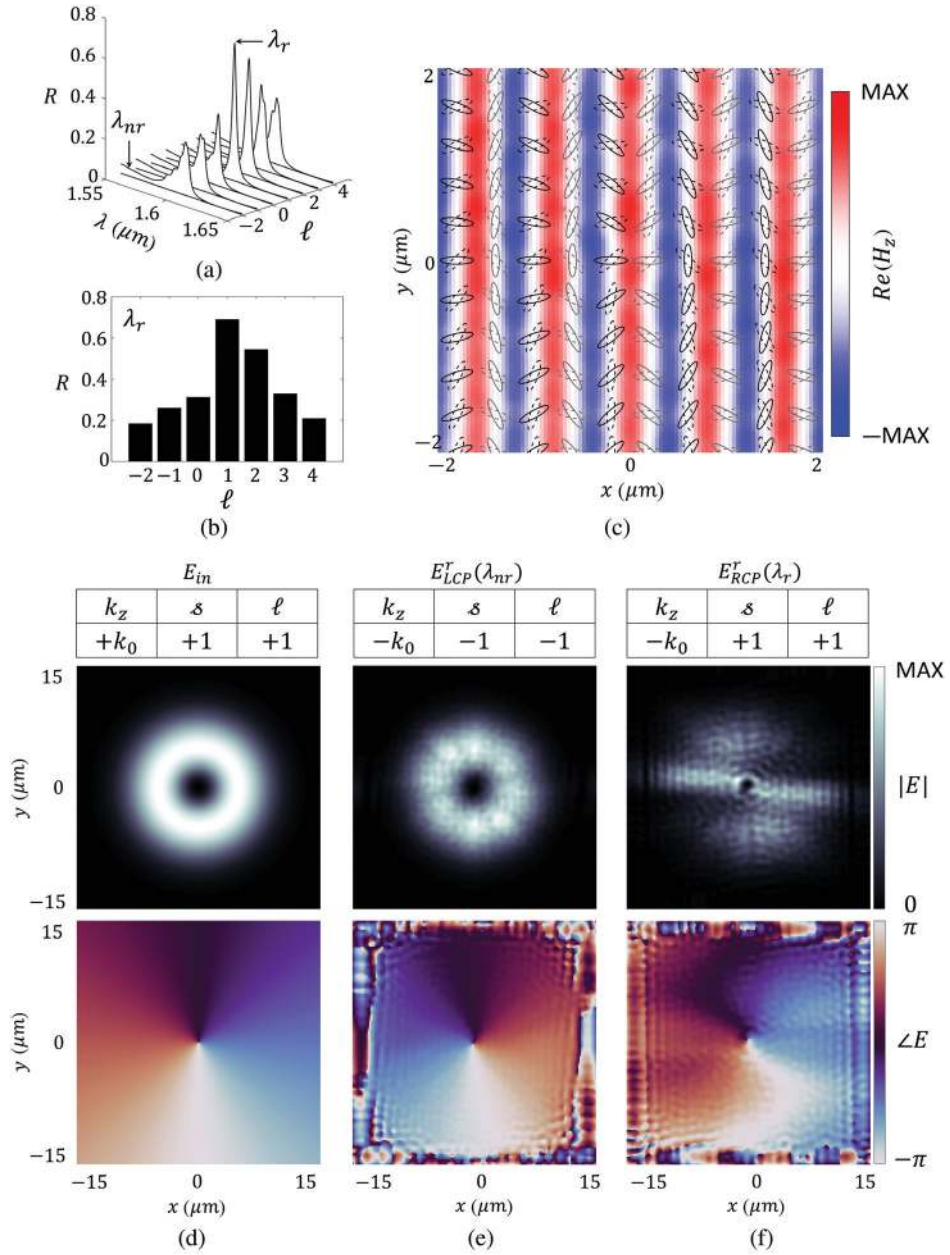

Fig. 5 Eigenwaves selective to both SAM and OAM. (a) Reflectance spectra for a range of OAM orders ℓ incident on a metasurface encoding a phase profile $\Phi = 2m \arctan 2(y, x)$. (b) Histogram showing the reflectance at the band-edge resonant wavelength λ_r, as a function of ℓ. (c) Field profile of the q-BIC illuminated by its eigenwave ($\ell = 1$) near the center of the device (which has a total aperture 30×30 μm); device geometry is overlaid with every other subperiod grayed out for clarity. (d) Incident electric field profiles with momenta tabulated (s denoting SAM). (e) Reflected beam at a non-resonant wavelength λ_{nr}, showing conventional specular reflection, with sign inversion for all momenta. (f) Reflected beam at the resonant wavelength λ_r, showing preservation of SAM and OAM.

its momenta. As reported in Figs. 5(a) and 5(b), when this eigenwave impinges on the device, a Fano resonance with large peak reflectance is observed, but for any other values of ℓ, the peak reflectance is reduced. This q-BIC metasurface, therefore, supports an OAM-selective Fano resonance.

As seen in Fig. 5(c), near the center of the device, the excited q-BIC has no residual phase profile, matching closely the expected profile of this mode. When light matching the eigenwave is incident [Fig. 5(d)], the amplitude and phase reflected at a non-resonant wavelength [shown in Fig. 5(e)] have all momenta inverted, as expected for specular reflection. The amplitude and phase of the reflected light at the resonant wavelength/wavefront, on the other hand, preserve both SAM and OAM [Fig. 5(f)].

We note that the Fano resonances in Figs. 3–5 do not have ideal unity diffraction efficiencies because their size is too small compared to the localization of energy in the q-BIC metasurface. The spatial profiles in Eq. (4) (and, in particular, the amplitude profile) must vary adiabatically relative to the characteristic lateral distance that the optical energy travels while resonating, otherwise, the interference of optical energy producing the Fano resonance will not be complete. The degree of lateral localization and the optical lifetime of the q-BIC, therefore, constrain the range of spatial frequencies an eigenwave can carry if near-unity diffraction efficiency is desired in a compact device.[14,35] Achieving flatter bands or using lower Q will improve the efficiency of the device within a finite range of spatial frequencies. q-BICs in high-contrast systems have been shown to enable flat bands with high Q-factor resonance,[35,36] offering precisely the needed degrees of freedom. However, as we have shown, such a choice will also decrease the spatial selectivity of the device. Alternatively, devices with larger footprint will achieve diffraction efficiencies approaching unity without altering the spatial selectivity. For instance, the 150-μm wide lensing device in Fig. 3(a) has a higher peak reflectance (90%) than the 50-μm device in Fig. 4(c) (70%), even though they have an identical numerical aperture, NA ≈ 0.48. We finally note that the reflected amplitude profile in Fig. 5(f) is distorted relative to the eigenwave; these distortions are due to the anisotropy of the band structure of the q-BIC, meaning the non-idealities related to band flatness apply inconsistently with respect to the in-plane directions. Future work developing a coupled mode theory describing these devices in the space-frequency domain will provide quantification and clarification of these limitations regarding band flatness and Q-factor.

We also note that both the periodic devices in Fig. 2 retain near-unity efficiency even when excited by plane waves other than the eigenwave at frequencies satisfying the dispersion relations [Eqs. (9) or (12)]. Yet, these modes do not reflect to time-reversed copies, as in the case of the band-edge. [Rather, as shown in Fig. 2(f), they are anomalously reflected in the general case of a phase gradient.] In this regard, these cannot be considered eigenwaves in the sense defined here. However, the time-reversed copy of the anomalously reflected plane wave must reflect to the original exciting plane wave. Hence, a superposition of these two plane waves can be considered the eigenwave in the sense considered here, reflecting to its time-reversed copy mediated by excitation of two counter-propagating q-BICs. This suggests that the aperiodic devices will also exhibit spatial selectivity off the band-edge to wavefronts produced by the interference of the two counter-propagating modes at frequencies off the band-edge. In this regard, our results can be seen as the scenario in which the counter-propagating modes unify into a single q-BIC at the band edge. Future work will explore the response of aperiodic Fano resonant metasurfaces off the band-edge frequency; this work is instead focused on establishing how the q-BIC symmetries alter the essential features of the band-edge mode in a way that translates the usual momentum-frequency selectivity into space-frequency selectivity.

4 Discussion

The results reported here demonstrate that chiral q-BICs with spatially tailored eigenpolarizations are characterized by an eigenwave that reflects with preserved handedness. In the case of a linear phase gradient, the consequence of preserving the handedness is retroreflection. The rule that the incidence angle is equal to the angle of reflection holds as usual, but with respect to a coordinate system of preserved handedness instead of inverted handedness. Our demonstrated Fano metalens may be thought of as a retroreflector with an angle that continuously varies across the device, demonstrating that this handedness preservation applies to eigenwaves spanning a range of spatial frequencies. Finally, the vortex beam Fano metasurface in Fig. 5 may also be described as a series of linear phase gradients wrapped azimuthally, locally retroreflecting the eigenwave. This azimuthal retroreflection has the consequence of preserving OAM when excited by the eigenwave.

The proposed scheme, therefore, enables an implementation of Fano metasurfaces that prescribes arbitrary spin, and spectral and spatial selectivity to an optical resonance. By tuning their chirality through $\Delta\alpha$, the spin selectivity may be arbitrarily tuned.[26] By tuning the magnitude of the perturbation $\delta = D_1 - D_2$, the spectral selectivity may be also widely controlled (the Q-factor varies as $Q \propto 1/\delta^2$).[13,14] By tuning the geometric phase, spatial wavefront selectivity is readily achieved by varying the deflection angle of the underlying angularly selective Fano resonance. Only the eigenwave precisely satisfies the angular selectivity at every location along the nonlocal metasurface. Band structure engineering may tune the degree of spatial selectivity.

Finally, we comment briefly on the role of the proposed chiral q-BIC platform (based on the approach introduced in Ref. 26) for demonstrating these concepts, and how our results differ from previously known phenomena in metasurfaces. Huygens' metasurfaces[37] are a well-known approach to achieve robust and highly efficient control of transmitted wavefronts, even including asymmetric and chiral responses.[38–40] By their nature, Huygens' metasurfaces are perfectly matched only at a single frequency, suggesting a degree of frequency selectivity in the wavefront transformation and the possibility of extending our results to transmissive type devices. Indeed, two Fano resonances may be tailored to interfere in a manner mimicking a Huygens' metasurface if the modes involved have opposite decay symmetry,[41] suggesting that this may even be done using the q-BIC mechanism. However, so far, Huygens' metasurfaces have not been explored in the context of sharp space-frequency selectivity. Regardless, such a system differs notably from our platform in that it relies on accidental (in contrast to symmetry-protected) spectral interference of two modes that are controlled by geometric parameters, while our platform manipulates the symmetries of a single-nonlocal mode responsible for the entire metasurface response. In other words, in the proposed platform, the wavefront-selectivity is an intrinsically encoded property of the band-edge mode itself, rather than a property of the interference of two leaky modes.

Similarly, a degree of frequency selectivity and angular selectivity is well-known to exist in conventional local metasurfaces, in that they only operate ideally for a single wavelength and angle of choice (see, for instance, Ref. 42). Often, it takes a concerted effort to reduce this selectivity in order to increase the bandwidth[43] or angular tolerance[44] of the wavefront transformation. However, in comparison to our structures, the bandwidth of these devices is much larger (by orders of magnitude), and this selectivity is very small due to the highly localized response of the metasurface scattering events. The difference is not simply in the degree of selectivity, but also in its form: in the q-BIC platform, the broadband local response (the continuum of states) is unaffected to the first order by the perturbation,[14] whereas the

discrete nonlocal response is arbitrarily tailored via the q-BIC symmetry properties. This feature results in a Fano resonance with in principle arbitrary Q-factors,[13] while conventional local metasurfaces cannot be described by Fano interference and do not have rationally controllable linewidths.

5 Conclusion

We have shown that metasurfaces with engineered q-BICs can support generalized Fano resonances that are selective to the shape of the incoming wavefront. When illuminated by their eigenwaves, the nonlocal band-edge mode is uniformly illuminated across the device, and the devices reflect light described by a coordinate system of preserved handedness; other excitations lead to weak responses and nearly full transmission. Our results extend the concept of Fano resonant metasurfaces from the momentum-frequency domain to the space-frequency domain, and the proposed design platform greatly advances the control over optical wavefronts and implements key functionalities for the growing fields of augmented reality and secure communications. Although we focused here on scalar wavefronts, we note that the present concept may, in principle, be extended one step further, such that nonlocal metasurfaces are selective to a vector beam excitation, i.e., a wavefront whose polarization state varies spatially. This opens the door to experimental demonstration of these concepts within single-layer devices,[28] wherein the linear polarization varies spatially, e.g., Fano resonant metasurfaces selective to a radially polarized beam. Beyond initial experimental verifications, we also envision interesting opportunities for these concepts in the context of thermal emission engineering. By considering the presence of small material loss in the proposed metasurfaces, we expect the emergence of a Lorentzian absorption peak with highly unusual wavefront and frequency selectivity. Due to the modal radiation laws,[45] this implies the possibility of tailoring the thermal emission with arbitrary wavefront selectivity based on these principles. A detailed discussion of these opportunities goes well beyond the scope of this paper, but this discussion highlights the rich phenomena unveiled by our findings in the context of generalized Fano responses with arbitrary wavefront selectivity, with a broad range of implications in several physics and engineering application areas.

Acknowledgments

This work was supported by the Air Force Office of Scientific Research MURI Program, the National Science Foundation EFRI program, and the Simons Foundation. The authors would like to acknowledge helpful conversations with Nanfang Yu and Stephanie Malek. The authors declare no conflicts of interest.

References

1. M. F. Limonov et al., "Fano resonances in photonics," *Nat. Photonics* **11**(9), 543–554 (2017).
2. U. Fano, "Effects of configuration interaction on intensities and phase shifts," *Phys. Rev.* **124**(6), 1866–1878 (1961).
3. R. W. Wood, "XLII. On a remarkable case of uneven distribution of light in a diffraction grating spectrum," *London Edinburgh Dublin Philos. Mag. J. Sci.* **4**(21), 396–402 (1902).
4. A. Hessel and A. A. Oliner, "A new theory of Wood's anomalies on optical gratings," *Appl. Opt.* **4**(10), 1275 (1965).
5. S. S. Wang et al., "Guided-mode resonances in planar dielectric-layer diffraction gratings," *J. Opt. Soc. Am. A* **7**(8), 1470 (1990).
6. S. S. Wang and R. Magnusson, "Theory and application of guided-mode resonance filters," *Appl. Opt.* **32**(14), 2606–2613 (1993).
7. M. Grande et al., "Graphene-based perfect optical absorbers harnessing guided mode resonances," *Opt. Express* **23**(16), 21032–21042 (2015).
8. C. J. Chang-Hasnain and W. Yang, "High-contrast gratings for integrated optoelectronics," *Adv. Opt. Photonics* **4**(3), 379–440 (2012).
9. S. Fan, W. Suh, and J. D. Joannopoulos, "Temporal coupled-mode theory for the Fano resonance in optical resonators," *J. Opt. Soc. Am. A* **20**(3), 569–572 (2003).
10. C. W. Hsu et al., "Bound states in the continuum," *Nat. Rev. Mater.* **3**(9), 16048 (2016).
11. Z. Sadrieva et al., "Multipolar origin of bound states in the continuum," *Phys. Rev. B* **100**(11), 115303 (2019).
12. S. Li et al., "Symmetry-protected bound states in the continuum supported by all-dielectric metasurfaces," *Phys. Rev. A* **100**(6), 063803 (2019).
13. K. Koshelev et al., "Asymmetric metasurfaces with high-Q resonances governed by bound states in the continuum," *Phys. Rev. Lett.* **121**(19), 193903 (2018).
14. A. C. Overvig et al., "Selection rules for quasi-bound states in the continuum," *Phys. Rev. B* **102**(3), 035434 (2020).
15. J. W. Yoon, S. H. Song, and R. Magnusson, "Critical field enhancement of asymptotic optical bound states in the continuum," *Sci. Rep.* **5**(1), 18301 (2015).
16. C. Qui et al., "Active dielectric antenna on chip for spatial light modulation," *Sci. Rep.* **2**, 855 (2012).
17. A. Tittl et al., "Imaging-based molecular barcoding with pixelated dielectric metasurfaces," *Science* **360**(6393), 1105–1109 (2018).
18. K. Koshelev et al., "Nonlinear metasurfaces governed by bound states in the continuum," *ACS Photonics* **6**(7), 1639–1644 (2019).
19. J. S. Ginsberg et al., "Enhanced harmonic generation in gases using an all-dielectric metasurface," *Nanophotonics* **10**(1), 733–740 (2020).
20. K. X. Wang et al., "Fundamental bounds on decay rates in asymmetric single-mode optical resonators," *Opt. Lett.* **38**(2), 100–102 (2013).
21. A. C. Overvig, S. C. Malek, and N. Yu, "Multifunctional nonlocal metasurfaces," *Phys. Rev. Lett.* **125**(1), 017402 (2020).
22. A. V. Kondratov et al., "Extreme optical chirality of plasmonic nanohole arrays due to chiral Fano resonance," *Phys. Rev. B* **93**(19), 195418 (2016).
23. J. S. Eismann, M. Neugebauer, and P. Banzer, "Exciting a chiral dipole moment in an achiral nanostructure," *Optica* **5**(8), 954–959 (2018).
24. Y. Hwang et al., "Effects of fano resonance on optical chirality of planar plasmonic nanodevices," *ACS Photonics* **5**(11), 4538–4544 (2018).
25. F. Zhang et al., "All-dielectric metasurfaces for simultaneous giant circular asymmetric transmission and wavefront shaping based on asymmetric photonic spin-orbit interactions," *Adv. Funct. Mater.* **27**(47), 1704295 (2017).
26. A. C. Overvig, N. Yu, and A. Alù, "Chiral quasi-bound states in the continuum," *Phys. Rev. Lett.* **126**(7), 073001 (2021).
27. S. C. Malek et al., "Active nonlocal metasurfaces," *Nanophotonics* **10**(1), 655–665 (2020).
28. S. C. Malek et al., "Resonant wavefront-shaping flat optics," arXiv:2009.07054 (2020).
29. F. Aieta et al., "Aberration-free ultrathin flat lenses and axicons at telecom wavelengths based on plasmonic metasurfaces," *Nano Lett.* **12**(9), 4932–4936 (2012).
30. N. Yu et al., "Light propagation with phase discontinuities: generalized laws of reflection and refraction," *Science* **334**(6054), 333–337 (2011).
31. M. Mansouree et al., "Multifunctional 2.5D metastructures enabled by adjoint optimization," *Optica* **7**(1), 77–84 (2020).
32. Y. Zhou et al., "Multifunctional metaoptics based on bilayer metasurfaces," *Light Sci. Appl.* **8**(1), 80 (2019).

33. R. C. Devlin et al., "Arbitrary spin-to-orbital angular momentum conversion of light," *Science* **358**(6365), 896–901 (2017).
34. K. Chen et al., "Directional Janus metasurface," *Adv. Mater.* **32**(2), 1906352 (2020).
35. A. C. Overvig, S. Shrestha, and N. Yu, "Dimerized high contrast gratings," *Nanophotonics* **7**(6), 1157–1168 (2018).
36. H. S. Nguyen et al., "Symmetry breaking in photonic crystals: on-demand dispersion from flatband to Dirac cones," *Phys. Rev. Lett.* **120**(6), 066102 (2018).
37. M. Chen et al., "Huygens' metasurfaces from microwaves to optics: a review," *Nanophotonics* **7**(6), 1207–1231 (2018).
38. C. Pfeiffer et al., "High performance bianisotropic metasurfaces: asymmetric transmission of light," *Phys. Rev. Lett.* **113**(2), 023902 (2014).
39. V. S. Asadchy et al., "Broadband reflectionless metasheets: frequency-selective transmission and perfect absorption," *Phys. Rev. X* **5**(3), 031005 (2015).
40. F. S. Cuesta et al., "Planar broadband Huygens' metasurfaces for wave manipulations," *IEEE Trans. Antennas Propag.* **66**(12), 7117–7127 (2018).
41. W. Suh, Z. Wang, and S. Fan, "Temporal coupled-mode theory and the presence of non-orthogonal modes in lossless multimode cavities," *IEEE J. Quantum Electron.* **40**(10), 1511–1518 (2004).
42. M. Khorasaninejad et al., "Metalenses at visible wavelengths: diffraction-limited focusing and subwavelength resolution imaging," *Science* **352**(6290), 1190–1194 (2016).
43. S. Shrestha et al., "Broadband achromatic dielectric metalenses," *Light Sci. Appl.* **7**(1), 85 (2018).
44. A. Arbabi et al., "Miniature optical planar camera based on a wide-angle metasurface doublet corrected for monochromatic aberrations," *Nat. Commun.* **7**(1), 13682 (2016).
45. D. A. B. Miller, L. Zhu, and S. Fan, "Universal modal radiation laws for all thermal emitters," *Proc. Natl. Acad. Sci. U. S. A.* **114**(17), 4336–4341 (2017).

Adam Overvig received his BS degree in engineering physics from Cornell University in 2013 and his PhD in applied physics from Columbia University in 2020. He is a postdoctoral researcher at the Advanced Science Research Center of the City University of New York. His current research interests include local and nonlocal metasurfaces, symmetries in optical devices, holography, and thermal photonics.

Andrea Alù received his Laurea degree in 2001 and his PhD in 2007 from the University of Roma Tre, Rome, Italy, and, after a postdoc at the University of Pennsylvania, he joined the faculty of the University of Texas at Austin in 2009, where he was the Temple Foundation Endowed Professor until January 2018. He is the founding director of the Photonics Initiative at the Advanced Science Research Center and the Einstein professor of physics at the Graduate Center of the City University of New York. He is a fellow of NAI, IEEE, AAAS, OSA, SPIE, and APS and has received several scientific awards, including the NSF Alan T. Waterman Award, the DoD Vannevar Bush Faculty Fellowship, the IEEE Kiyo Tomiyasu Award, the OSA Adolph Lomb Medal, the ICO Prize in Optics, the TAMEST Award in engineering, and the URSI Issac Koga Gold Medal.